Estimation of Left Ventricular Mass and Infarct Size from Nitrogen-13-Ammonia PET Images Based on Pathological Examination of Explanted Human Hearts

Dominique Delbeke, Christine H. Lorenz, John R. Votaw, Susan T. Silveira, William H. Frist, James B. Atkinson, Robert M. Kessler and Martin P. Sandler

Departments of Radiology, Cardiothoracic Surgery and Pathology, Vanderbilt University Medical Center, Nashville, Tennessee

The purpose of this study was to develop a technique to quantify left ventricular mass and infarct size in chronic ischemic heart disease from PET images based on correlation with pathological examination of explanted human hearts. Fourteen hearts from patients with cardiomyopathy who had ^{13}N-ammonia scans prior to orthopic heart transplantation were studied. Accurate estimation of the *relative* infarct size was possible in patients with a well-delineated, nearly transmural infarct ($r = 0.93$, $y = 1.1x - 0.7$, $n = 11$). Both *absolute* and *relative* infarct mass measurements on PET images correlated well with pathological measurements. We identified a population of patients with patchy interstitial or subendocardial scarring with globally reduced perfusion, for which the infarct size could not be estimated using the criteria derived for the patients with well-delineated infarcts.

J Nucl Med 1993; 34:826–833

The ability to measure myocardial infarct size may have prognostic significance in patients with coronary artery disease (*1–4*) and quantification of left ventricular mass may be clinically important in patients with cardiac hypertrophy (*5*). Several studies have shown that the left ventricular mass and myocardial infarct size can be estimated using ^{201}Tl single-photon emission tomography (SPECT) (*6–11*). However, ^{201}Tl has technical limitations due to low photon energy (70 keV) which is suboptimal for detection by current gamma cameras, and a long half-life which precludes administration of high doses. Recently, ^{99m}Tc-labeled agents, such as ^{99m}Tc-2-hexakis-2-methoxy-2-methylpropyl-isonitrile (sestamibi), have become available and their applicability for quantification of myocardial infarction and myocardial salvage after reperfusion has been investigated in both animal models and humans (*12,13*). The better resolution of positron emission tomography (PET) when compared to conventional SPECT (7.5 mm versus 14 mm) should improve the accuracy of scintigraphic imaging to noninvasively quantitate myocardial infarct size and myocardial mass. In addition, PET allows correction for photon attenuation that creates artifacts in SPECT studies.

Thallium-201, ^{99m}Tc-isonitriles SPECT data and ^{11}C-palmitate PET data with pathological correlation have been obtained in the canine model with experimentally-induced acute myocardial infarction (*6–9,12,14*). Studies performed in humans have evaluated left ventricular mass and correlated scintigraphic data with angiography (*10*). Infarct size in humans evaluated with ^{201}Tl and metabolic PET imaging using ^{11}C-palmitate has been correlated with creatine kinase released into the bloodstream (*11,15*) and validated with phantom studies (*13*). A recent study in humans attempted to estimate infarct size by using ^{18}F-fluorodeoxyglucose images and comparing these estimates with infarct size measured using ^{82}Rb images, an agent which evaluates cell membrane integrity (*16*). No pathological correlation was obtained in these human studies (*10,11,13,15,16*).

PET technology may be more clinically useful in chronic ischemia than acute infarction because of the problems in transporting unstable patients outside the intensive care unit. The purpose of this study was to develop a technique to quantify left ventricular mass and infarct size from PET images in humans with chronic ischemic heart disease. We estimated left ventricular mass and infarct size from ^{13}N-ammonia PET images in 14 patients with cardiomyopathy scheduled for heart transplantation and compared the findings with pathological measurements of the explanted hearts.

Received Jun. 18, 1992; revision accepted Nov. 5, 1992.

For correspondence or reprints, contact: Dominique Delbeke, MD, Department of Radiology, Vanderbilt University Medical Center, 21st and Garland Ave., Nashville, TN 37232.

MATERIALS AND METHODS

Patient Population

We studied 14 patients who underwent PET imaging prior to cardiac transplantation. There were 13 males and one female aged 32–59 yr. The average time between PET imaging and transplantation was 86 ± 67 days (mean ± s.d.). There were no clinically significant intervening cardiac events between the time of PET imaging and cardiac transplantation. Thirteen patients had ischemic cardiomyopathy and one patient had radiation-induced cardiomyopathy following mediastinal irradiation for Hodgkin's disease. The patient with radiation-induced cardiomyopathy was included as a control with 0% infarct.

PET Imaging

PET was performed with a Siemens ECAT 933/08/16 tomograph (Siemens Medical Systems, Inc., Hoffman Estates, IL) with the patient at rest. The tomograph had 8 detector rings to collect 15 transaxial images. The sensitivity as measured by scanning a 20-cm diameter cylindrical uniform phantom was 13,000 cps/mCi/ml in the direct planes (1, 3, 5 . . . 15) and 23,000 cps/mCi/ml in the cross planes. The axial field of view was 12.8 cm, the intrinsic resolution was 4.8 mm at the center of the field of view and the reconstructed resolution was 7.5 mm (FWHM). There was an average of 2.5 million true counts per image. The scanner hardware estimates and corrects for random events using the standard delayed window technique. Electrocardiographic gating was not employed.

Transmission images were obtained to correct for photon attenuation. Without moving the patient, dynamic image collection was started coincident with intravenous administration of 20 mCi of ^{13}N-ammonia. The dynamic sequence typically consisted of a 4-min image mainly for blood-pool information, followed by a 15-min image for measuring tissue activity distribution (*17*). Because of the retrospective aspect of this study, rapid sequential data frames, as described in the recent literature (*18*), were not available for all patients to calculate absolute flow values on early data frames; therefore, the 4-min to 19-min images were analyzed in this study. Calculation of left ventricular mass and infarct mass was performed on relative estimates of perfusion. The late images have been shown to give more variable estimates of the net ^{13}N-ammonia extraction because of continuous myocardial uptake or clearance of ^{13}N activity over time (*18*).

Image volume was reoriented along the short-axis of the heart in 1-cm thick slices. From the axial views, vertical long-axis views were obtained by drawing an axis from the middle of the apex to the middle of the base of the left ventricle. Then, on the vertical long-axis views, an axis was drawn from the middle of the apex to the middle of the base and short-axis views were generated by slicing the image of the heart perpendicular to that vertical long-axis. All slices from the base to the apex were analyzed to determine left ventricular mass. The apex was defined as the most apical slice where the ventricular cavity could still be identified. The base of the heart was defined as two slices above the membranous septum. The two slices with membranous septum were not included in the analysis of infarct mass determination. Analysis of these short-axis images was performed as described below.

Pathological Examination of the Explanted Hearts

Immediately after surgical removal, the explanted hearts were cut parallel to the atrioventricular sulcus into 1-cm thick slices from the apex to the base. To exclude a recent acute myocardial infarction, the slices were then stained by the triphenyltetrazolium chloride technique, a tissue enzyme stain which forms a red precipitate in the presence of intact dehydrogenase activity and therefore identifies viable myocardium (*19*). Each slice was incubated in a prewarmed (37°C) fresh 1% solution of triphenyltetrazolium chloride in Trizma buffer solution for 15 min. Two hearts were not available for examination until the day after surgery and were not stained; they were included in the study because all patients studied had old infarcts and the scarred areas were easily identifiable with or without triphenyltetrazolium chloride stain. The history of these two patients did not suggest any recent acute cardiac event.

Following staining, the apical and basal surfaces of each slice were photographed. The right ventricular free wall and papillary muscles, epicardial fat and valves were excised and the left ventricular portion of each slice was weighed. The weight of the left ventricle is referred to as the actual left ventricular mass. The actual left ventricular mass ranged from 97 to 391 g (mean ± s.d. = 242 g ± 74, n = 14). The specimen was then fixed in formalin.

The left ventricular mass and infarct mass were measured by computer-assisted planimetry of enlarged photographs of both sides of each myocardial slice. The planimetric delineation of the infarcted areas was possible in patients with transmural infarcts. Three patients whose hearts exhibited patchy interstitial fibrosis could not be analyzed. The mass of each slice was calculated by averaging the apical and basal surfaces and multiplying this surface by the thickness of the slice (1 cm) and the assumed specific density of the myocardium (1.05 g/cm^3). To our knowledge, the specific gravity of scar tissue is not known. The left ventricular mass measured by planimetry was obtained by summing the left ventricular mass of each slice. The absolute infarct mass was calculated by multiplying the percentage of infarcted surface in that slice by the weight of that slice and summing the absolute myocardial infarct mass of each slice. The relative infarct mass was calculated by dividing the absolute infarct mass by the actual left ventricular mass.

The planimetric measurements were validated by comparing the actual left ventricular mass obtained by gravimetry to the left ventricular mass measured by planimetry. The linear regression analysis yielded the following relation: planimetric mass (g) = 0.88 × gravimetric mass + 4.0, with a strong correlation (r = 0.97, n = 14). The standard error of the planimetric mass estimates was 16.3 g and was probably due to variation in thickness of the slices because accurate slicing of fresh hearts is difficult. However, the thickness of the slices should not affect the pathological estimates of the infarct size because the percentage of infarcted surface in each slice was multiplied by the actual mass of the slice.

Analysis of ^{13}N-Ammonia Scans

Semi-automated Edge Detection and Sector Analysis. Analysis of the short-axis PET images was performed on a MicroVAX II computer (Digital Equipment Corp., Maynard, MA) with a commercial image display board (Data Translation, Marlboro, MA). A software program using a previously published semi-automated edge detection algorithm (*20,21*) was designed and implemented to define the epicardial and endocardial borders of the left ventricle. In this program, the operator chooses a center point inside the left ventricular cavity and an outer limit point outside the left ventricle. The subsequent search for edges

is confined to the interior of the circle defined by these two points. Each image is then converted to polar coordinates along 36 equidistant radii. The first and second derivatives are computed along each ray and a cost matrix is defined as the inverse of the second derivative (*20,21*). Two minimal cost paths are found through this matrix corresponding to the endocardial and epicardial edges. The contours are then converted back into the cartesian frame and the edges are displayed. The user has the option of moving any of the edge points placed incorrectly by the algorithm. The number of edge points initially placed incorrectly by the automatic algorithm and corrected by the user was high (up to 50%) in patients with patchy uptake, but was insignificant (< 15%) in patients with a well delineated defect. In all cases, the points that were placed correctly by the algorithm served as a guiding contour for manual correction of the remaining edge points.

In order to reduce the effect of fluctuations of counts per voxel in single voxels, the average counts per voxel are calculated in each of 36 circumferential sectors per image. For simplicity, these values are hereafter referred to as sector values. Each sector typically contained 15–20 voxels. The maximum sector value was determined for each slice and stored for further analysis. The left ventricular mass was calculated from the total number of voxels in all slices of the heart and multiplied by the volume of each voxel and the assumed specific density of the myocardium, 1.05 g/cm^3.

Determination of Infarct Threshold and Infarct Size Estimation. To identify the volume of infarcted myocardium, a thresholding technique was used to identify sectors with low perfusion. The goal was to define a criterion derived from the images that could be universally applied to the entire set of patients.

In order to evaluate the sensitivity of infarct size estimation on thresholding, the percent infarct was calculated for a range of thresholds from 0% to 100% of the maximum sector value. Figure 1 shows the relationship between threshold and calculated infarct for a typical patient study. Since the relationship is sigmoidal, a small change in threshold at low thresholds results in only small changes in calculated infarct size. However, in the middle range of thresholds, any small change in threshold results in a large change in the calculated infarct size. Because of this high sensitivity to choice of threshold, any parameter used to determine a threshold for infarct size must be relatively insensitive to noise. Therefore, the choice of parameter on which to base threshold definition must reduce noise while maintaining the ability to discriminate between small differences in actual infarct size.

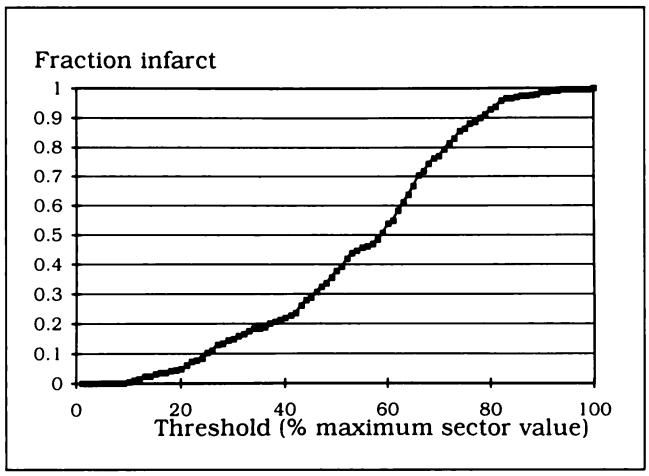

FIGURE 1. Graph representing a typical example of the fraction infarct calculated on PET images by choosing different thresholds (expressed in % maximum sector value in the heart) to define infarcted from normal myocardium. A small change in threshold results in a large change in estimated infarct size.

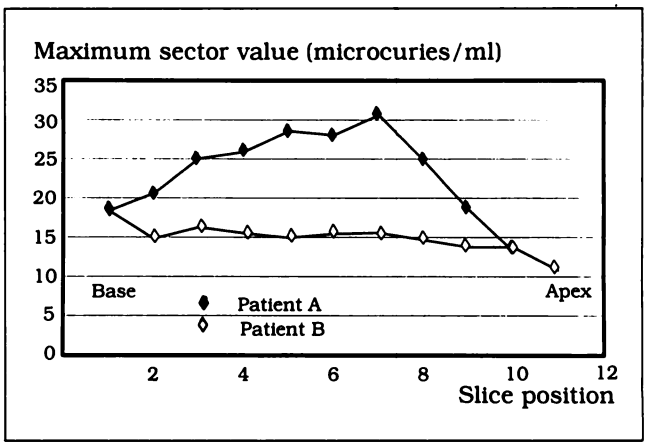

FIGURE 2. Graph showing typical examples of maximum sector value per PET slice plotted against the slice position in the heart of a patient with transmural infarction (A) and (B) a patient with patchy fibrosis.

As previously mentioned, the purpose of the study was to find a parameter derived from each individual's PET images that would accurately predict infarct size. The following approach was used to define the most appropriate threshold for identifying infarcted myocardium: (1) identify a parameter (e.g., the maximum sector value in each heart), (2) calculate the percent magnitude of that parameter that would yield the infarct size determined by planimetry for each heart and (3) evaluate the derived threshold for consistency in infarct size prediction over the entire patient group.

Figure 2 shows the maximum sector values plotted against the slice position in the heart for two of the patient studies. Most hearts displayed the pattern shown in curve A, with a tapering of maximum sector values at the apex and base. Hearts with patchy scarring typically showed the pattern in curve B, with low perfusion throughout. Choosing a single sector with the highest sector value in an entire heart as a basis for threshold determination yielded variable results when calculating infarct size. To reduce this variability, the average of the maximum sector values from each slice was used as the parameter on which to base threshold determination. For this group of patients, excluding those with patchy scarring, the optimum threshold was found to be 60% of the average maximum sector value.

Using this threshold, the absolute infarct mass was then estimated from the number of voxels in all slices that had mean counts per voxel below the derived threshold, multiplied by the volume of each voxel and the assumed specific density of the myocardium.

Statistical Methods

Actual and PET-estimated left ventricular mass and infarct mass were compared using linear regression analysis and correlation coefficients for paired data.

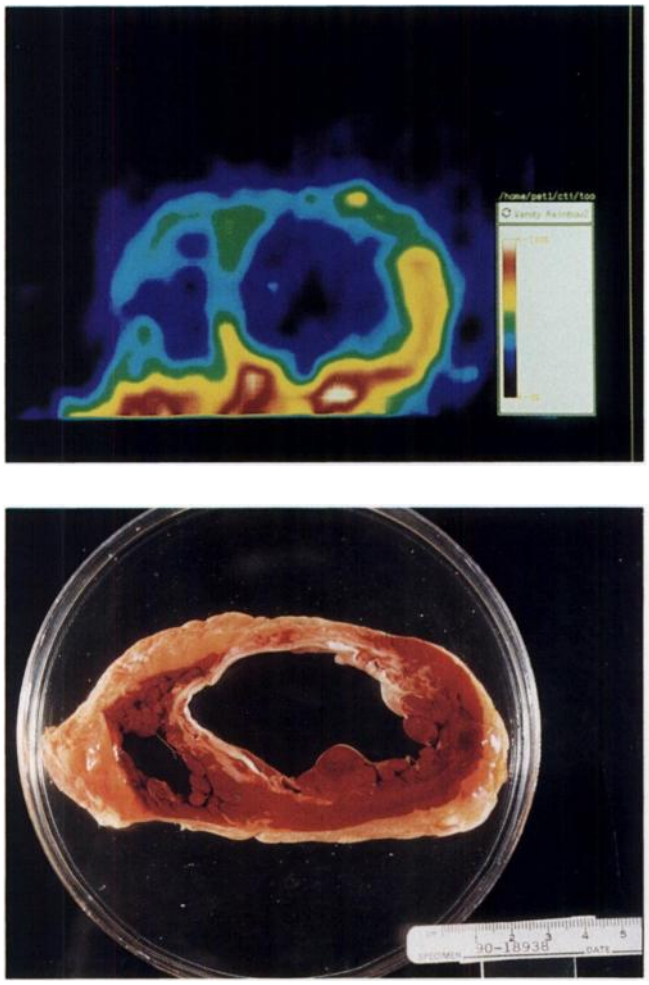

FIGURE 3. Images showing activity distribution of ^{13}N-ammonia 4 to 19 min postinjection in a 57-yr-old patient with a history of previous myocardial infarction and ischemic cardiomyopathy. The top of the color scale represents the highest activity in the image. (Top) Short-axis images from the mid-heart show a ^{13}N-ammonia defect in the anterior wall of the left ventricle corresponding to (bottom) an old transmural infarct seen on the pathological specimen.

RESULTS

Visual Comparison of PET Images and Pathological Specimens

By visual inspection, defects on ^{13}N-ammonia scans corresponded to scarred tissue on the pathological specimen in all patients. The defects were easily delineated in patients who had a predominantly transmural infarct (Fig. 3). These patients had marked thinning of the myocardial wall in the infarcted areas and markedly reduced perfusion on PET images. Other patients had smaller areas of transmural infarct surrounded by large areas of subendocardial infarcts. The ^{13}N-ammonia activity present appeared proportional to the thickness of preserved myocardium. Delineation of the infarct was more difficult but still possible in these patients both pathologically and on the PET images. However, three patients had patchy interstitial fibrosis located predominantly in one vascular territory in the basal and mid-portion of the heart extending circumferentially toward the apex (Fig. 4). The thickness of the myocardial wall was only somewhat reduced, and pathological delineation of the infarcted areas was difficult and subjective in these cases. These patients had reduced perfusion in most of the myocardium and a defect could not be easily delineated visually. The patient with radiation-induced cardiomyopathy had normal PET images and the pathological examination was normal, with homogenous red coloration by triphenyltetrazolium chloride stain, compatible with viable myocardium. Microscopically, there was epicardial, endocardial and perivascular fibrosis, findings typical of radiation-induced damage.

Intraobserver and Interobserver Variability

All ^{13}N-ammonia images were analyzed by two independent observers to determine interobserver variability. All were analyzed a second time by one of the observers

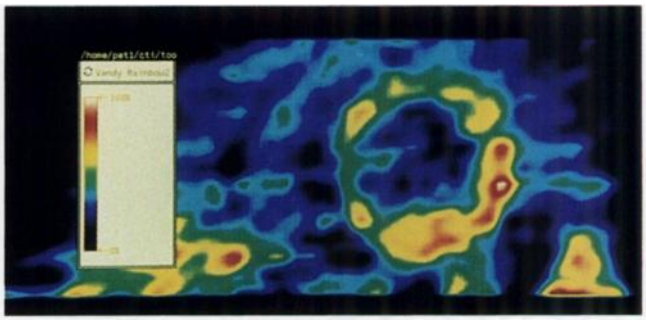

FIGURE 4. Images showing activity distribution of ^{13}N-ammonia 4 to 19 min postinjection in a 58-yr-old patient with a history of ischemic cardiomyopathy. The top of the color scale represents the highest activity in the image. (Top) Short-axis images from the mid-heart show globally decreased perfusion on the ^{13}N-ammonia scan corresponding to (bottom) patchy interstitial fibrosis mostly in the anterolateral wall of the left ventricle and extending circumferentially in most apical slices. Myocardial wall thickness is better preserved than in the patient shown in Figure 3.

TABLE 1
Parametric Values Determined by Each Observer

Patient	Left ventricular mass (g)			Absolute infarct mass (g)			Relative infarct mass (%)		
	obs1 A	obs1 B	obs2	obs1 A	obs1 B	obs2	obs1 A	obs1 B	obs2
FL	406	446	482	62	71	45	14	16	9
KM	519	488	533	137	123	146	26	25	27
SG	493	546	566	117	153	108	24	28	19
CF	517	548	584	307	285	239	54	52	41
JD	772	857	870	206	183	239	24	21	28
LC	524	522	553	175	186	159	33	36	29
WB	566	535	587	165	170	176	29	32	30
DD	586	578	612	22	25	18	4	4	3
JS	576	689	657	130	173	115	23	25	19
MF	492	518	482	177	207	193	40	40	39
WK	938	890	884	329	350	333	35	39	38
EH	385	363	384	80	68	70	21	19	18
EN	689	641	740	64	103	104	9	16	14
BW	442	363	443	4	15	3	1	4	1

to determine intraobserver variability. Good interobserver and intraobserver agreement was found, which demonstrates the reliability of the edge detection algorithm. Although the percent infarct size determined for the patients with patchy fibrosis was inaccurate, it was highly reproducible. Table 1 lists the values found by each observer for left ventricular mass, absolute infarct mass, and relative infarct mass for the fourteen patients. Table 2 summarizes the interobserver and intraobserver analysis. The mean difference between observers for the group is shown in both absolute and percentage terms. The variability, defined as the standard deviation of the difference between observers, is also shown in both absolute and percentage terms. Linear regression analysis comparing pairs of observers yielded the correlation coefficients listed in the table.

Quantitative Comparison of Left Ventricular Mass and Infarct Size Determined on PET Images and the Pathological Specimen

The left ventricular mass measured on ^{13}N-ammonia images was compared with the actual mass measured by gravimetry. Although the correlation coefficient was 0.82 for 14 hearts, PET overestimated the left ventricular mass approximately two-fold (Fig. 5). This overestimation is most probably due to partial volume averaging and heart motion artifacts, which make discrimination between the true epicardial and endocardial edges and the visualized edges of the myocardium difficult to detect on PET images, especially in patients whose hearts exhibit areas of reduced uptake. When the three patients with patchy fibrosis and global diminished uptake were excluded, the correlation coefficient improved to 0.93 and the standard error to 61.5 g.

The three patients with patchy fibrosis and patchy reduced uptake of ^{13}N-ammonia were not included in the infarct size evaluation because the infarcted areas could not be easily delineated pathologically, nor could they be defined on PET images by the threshold chosen as described above. As expected, the absolute infarct mass was overestimated on PET images in the same proportion as the left ventricular mass because of the epicardial and endocardial edges' definition (Fig. 6A). However, the

TABLE 2
Results of Interobserver and Intraobserver Analysis

	Left ventricular mass (g)		Absolute infarct mass (g)		Relative infarct mass (%)	
	%	Absolute	%	Absolute	%	Absolute
Mean difference						
Interobserver	8	46	17	18	18	4
Intraobserver	8	44	23	20	20	3
Variability						
Interobserver	5	29	12	17	14	3
Intraobserver	5	30	29	13	32	2
Regression correlation coefficient						
Interobserver	n/a	0.95	n/a	0.96	n/a	0.95
Intraobserver	n/a	0.94	n/a	0.97	n/a	0.98

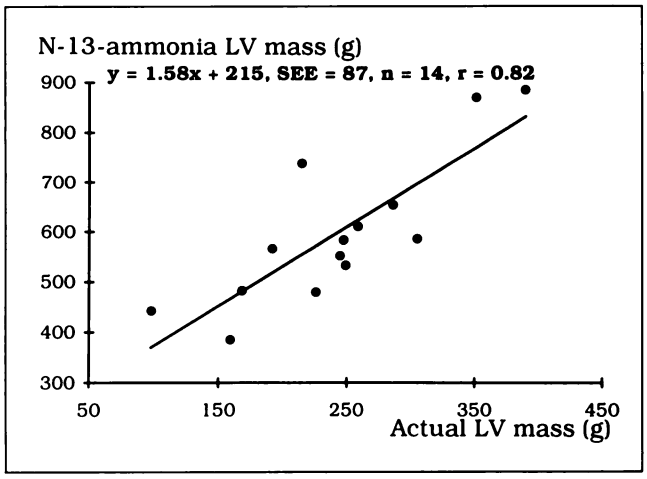

FIGURE 5. Correlation of ^{13}N-ammonia PET derived estimates of left ventricular mass with the actual left ventricular mass. The solid line is the linear regression between the two sets of values.

relative (percent) infarct mass was accurately measured compared to measurements on pathological specimens (Fig. 6B). Both absolute and relative infarct mass measurements on PET images correlated well with pathological measurements (r = 0.93).

DISCUSSION

PET is an established and reliable imaging modality for quantifying myocardial perfusion and metabolism in patients with a variety of acute and chronic cardiac diseases. However, techniques to quantify the mass of myocardium that is scarred or ischemic are not yet well defined. In this study, we developed a technique allowing measurement of infarct size with ^{13}N-ammonia PET images based on pathological measurements on explanted hearts of patients with cardiomyopathy.

Most studies using scintigraphic procedures to estimate infarct size express the infarct size relative to normal myocardial tissue. Numerous methodologies have been described, including circumferential profile analysis assuming constant wall thickness (*6*), maximum count circumferential profile analysis (*9,12,13,16*), edge detection algorithms to define the true endocardial and epicardial border of the myocardium (*7,8,10,14,15*) and definition of the endocardial and epicardial edges manually after subtraction of background activity present in the infarcted region (*11*). The infarct size has been estimated by drawing ROIs (*6*), calculating the percentage of pixels with uptake below a threshold within the boundaries of the left ventricle (*8,11–16*) and by calculating the percentage of maximum count circumferential profile points falling below normal values established by reference to a normal population or phantom studies (*9,13*). When quantification depends on circumferential profile analysis, the importance of correcting for the slice mass contribution to the left ventricular mass has been emphasized in the literature (*9*). We used a semi-automated edge detection program to delineate the endocardial and epicardial edges of the myocardium and found that in order to estimate the infarct size in this patient population, the most appropriate threshold was 60% of average maximum sector values of all slices in the heart.

Our study shows that by visual inspection, decreased perfusion is more severe in areas of transmural infarction than nontransmural infarction. This observation supports the data from Hashimoto et al. (*22*) showing that areas with decreased ^{13}N-ammonia uptake were present most frequently in patients with Q-wave myocardial infarction than in patients with non-Q-wave infarction. This is partially explained because PET cannot resolve subepicardial-subendocardial difference and shows mean transmural radionuclide distribution.

Although PET left ventricular mass correlated well with actual mass, ^{13}N-ammonia images overestimated the left ventricular mass and absolute infarct mass by approximately two-fold. The explanation for this overestimation can be divided into two main components. The first is the

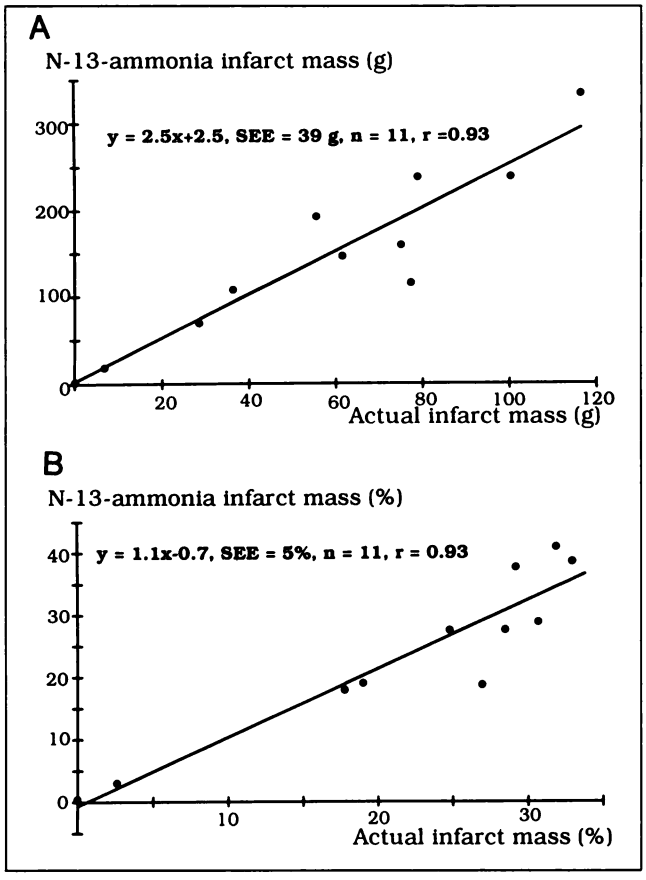

FIGURE 6. (A) Correlation of ^{13}N-ammonia PET derived estimates of the absolute infarct mass with the absolute infarct mass estimated by planimetry. The solid line is the linear regression between the two sets of values. (B) Correlation of ^{13}N-ammonia PET derived estimates of the relative (percent) infarct mass with the relative (percent) infarct mass estimated by planimetry. The solid line is the linear regression between the two sets of values.

contribution of motion artifacts and partial volume artifacts which is also a problem in SPECT imaging. The second is the choice of edge detection algorithm.

In this study, all of the images were nongated acquisitions of 15 min duration starting 4 min postinjection. To assess the activity in an anatomic structure by PET imaging, the sampled volume should exceed the physical dimension of the resolution element by a factor of two because of the partial volume effect (*23*). Although the thickness of the myocardium is less than 10 mm in infarcted areas, in most regions the thickness of the myocardium varies from 10 to 20 mm (Figs. 3 and 4). Because the reconstructed resolution of the scanner is 7.5 mm, heart motion probably causes greater artifacts in the images than partial volume effects. Motion reduces the clarity of the edges and increases the detected activity within the heart chambers. Activity will be detected from a volume that is larger than the actual volume of the heart. The contrast seen in infarcts is also reduced when tissue containing activity moves to a position formerly occupied by the infarct. Since the true activity is much greater in healthy tissue, the measured healthy tissue-to-infarct contrast can be much different than the true activity contrast. Subtracting a constant background from the images will alter the contrast and the apparent size of the imaged heart. The largest contributor to true background is scatter. Subtracting a background to correct for motion artifacts is seen as an arbitrary correction and, since an accurate estimate of scatter is not available, no background subtraction correction was made. Gating the acquisition would reduce these problems but because of the effects on infarct contrast, the threshold used to identify infarcted tissue would depend on the acquisition protocol. Gating these studies and redetermining a threshold is expected to produce more accurate results. The low count efficiency of ^{201}Tl makes it a suboptimal agent for acquiring gated cardiac images, but gated acquisition of ^{99m}Tc-sestamibi SPECT (*24*) and ^{13}N-ammonia PET images (*25,26*) have been described to evaluate myocardial wall thickening during the cardiac cycle. When the image acquisition is gated, the range of wall motion within a gated image is decreased and the walls appear thinner. Therefore, cardiac gating reduces artifacts due to motion at the expense of partial volume effects. Furthermore, because significant variation of wall motion still occurs during the gating intervals (approximately 150 msec), gated acquisition of PET images will partially, but not totally, correct for wall motion artifacts. The effects on the edge detection algorithm of wall motion and partial volume effects during gating are currently under investigation in our laboratory.

The second component contributing to the overestimation of myocardial mass and absolute infarct size is the choice of edge detection algorithm. Many choices for edge detection algorithms are available. A number of those used previously, such as the one used by Narahara et al. (*8*), make geometric assumptions concerning the left ventricle. We chose an algorithm that is not constrained by geometric assumptions. Although the algorithm we implemented yielded reproducible results, its tendency was to identify "loose" borders. These borders yielded a myocardial wall thickness of 1.5–2 times the actual thickness. Recognizing this problem, we could have chosen to artificially "tighten" the borders using a variety of methods, such as those used by researchers using SPECT to estimate myocardial mass and infarct size (*6–12*). However, we chose not to use any arbitrary means to reduce overestimation. In this study, we were primarily concerned with developing a method that would accurately measure infarct size and, secondarily, to accurately estimate left ventricular mass. Despite the overestimation, our method correlated highly with the actual measurements. A regression equation could be used to extract the absolute mass from the PET estimates, although it would not be ideal for practical use. Ideally, estimation of mass by PET should be accurate as well as highly correlated with actual mass. We are currently working on methods to modify the edge detection algorithm in a nonarbitrary manner to reduce the problem of overestimation.

We were able to accurately estimate the relative infarct size in a population of patients with remote infarcts using a threshold of 60% of average maximum sector values in the heart. This is close to the threshold of 55% of maximum ^{18}F-fluorodeoxyglucose activity used to define nonviable myocardium by Gould et al. (*16*) in a mixed population of patients with recent and old infarcts. These thresholds appear to be higher than the threshold chosen by others to measure acute infarct size with ^{201}Tl in the experimental dog model (*8*). This is probably because some areas of scarring are transmural in patients with multivessel chronic ischemic disease, but others are subendocardial or patchy and the thickness of the myocardium is variable. However, the thresholds derived from this study have been determined iteratively and are specific for this patient population. A prospective application of this technique to a subsequent group of patients is necessary for complete evaluation. Another limitation of this study is the average interval of 86 days between the PET scan and the pathological examination of the heart. In patients with coronary artery disease, intervening events can be clinically uncertain. However, in these patients, visual comparison of the PET imaging with the explanted hearts showed no evidence of additional infarction between the time of the PET scan and explantation.

The standard error of relative infarct size estimates in our study was 5%, which is similar to other findings (*8,9,12*). Multiple clinical studies have been performed evaluating the size of perfusion defects in acute myocardial infarction before and after reperfusion; they show a wide range of improvement after reperfusion with a mean reduction in defect size of 13% (*13*). Therefore, a 5% standard error on the accuracy of the relative infarct size measurements would be clinically acceptable.

SUMMARY AND POTENTIAL FUTURE APPLICATIONS

In this study, we were able to derive a threshold of ^{13}N-ammonia uptake (60% of average maximum sector values) that corresponds to actual infarcted myocardium on explanted hearts from patients with cardiomyopathy. By defining as infarcted myocardium the mass of tissue with uptake below that threshold, we could accurately measure the relative (percent) infarct size in patients with a well delineated transmural infarct (11/14 patients studied). We identified a population of patients with patchy myocardial fibrosis for which infarct size could not be evaluated using the criteria established for the patients with well delineated infarcts (3/14 patients studied). These patients had a patchy pattern of ^{13}N-ammonia uptake and could be easily identified by visual inspection of the images.

Most of the data in the literature about quantification of infarct size were obtained in acutely infarcted animal models, where there were optimal conditions (e.g., infarcted tissue was well delineated, the thickness of the myocardium was preserved and adjacent myocardium was totally free of disease). The results of this study emphasize that extrapolation of animal data to patients with chronic coronary artery disease should be done with caution.

In this study, a technique was developed to quantify defect size on ^{13}N-ammonia PET images. These defects corresponded to scarred myocardium in our patient population awaiting cardiac transplantation. If quantitative estimates of myocardial defect size can be performed with PET, a combined geometric analysis of perfusion defect and metabolic activity should help to quantify viable myocardium with decreased perfusion and metabolic activity, thereby determining which patients would most likely benefit from reperfusion by surgical revascularization or percutaneous transluminal procedures.

ACKNOWLEDGMENTS

The authors thank Marshall Watson for assistance with data analysis, John Bobbitt for assistance in preparing the illustrations and Virginia Brocker for careful preparation of the manuscript.

REFERENCES

1. Page DL, Caufield JB, Kastor JA, DeSanctis RW, Sanders C. Myocardial changes associated with cardiogenic shock. *N Engl J Med* 1971;285:133–137.
2. Alonso DR, Scheidt S, Post M, Killip T. Pathophysiology of cardiogenic shock. Quantification of myocardial necrosis: clinical, pathologic and electrocardiographic correlations. *Circulation* 1973;48:588–596.
3. Sobel BE, Bresnahan GF, Shell WE, Yoder RD. Estimation of infarct size in man and its relation to prognosis. *Circulation* 1972;46:640–648.
4. Silverman KJ, Becker LC, Bulkley BH, et al. Value of early thallium-201 scintigraphy for predicting mortality in patients with acute myocardial infarction. *Circulation* 1980;61:996–1003.
5. Pantely G, Morton M, Rahimtoola SH. Effects of successful, uncomplicated valve replacement on ventricular hypertrophy, volume and performance in aortic stenosis and in aortic incompetence. *J Thorac Cardiovasc Surg* 1978;75:383–391.
6. Keyes JW, Brady TJ, Leonard PF, et al. Calculation of viable and infarcted myocardial mass from thallium-201 tomograms. *J Nucl Med* 1981; 22:339–343.
7. Weiss RJ, Buda AJ, Pasyk S, O'Neill WW, Keyes JW, Pitt B. Noninvasive quantification of jeopardized myocardial mass in dogs using two-dimensional echocardiography and thallium-201 tomography. *Am J Cardiol* 1983;52:1340–1444.
8. Narahara KA, Thompson CJ, Maublant JC, Criley JM, Mena I. Estimation of left ventricular mass in normal and infarcted canine hearts using thallium-201 SPECT. *J Nucl Med* 1987;28:1315–1321.
9. Pringent F, Maddahi J, Garcia EV, Resser K, Lew AS, Berman D. Comparative methods for quantifying myocardial infarct size by thallium-201 SPECT. *J Nucl Med* 1987;28:325–333.
10. Narahara KA, Thompson CT, Maublant JC, Brizendine M, Mena I. Thallium-201 single-photon emission tomography estimates of left ventricular mass in patients with and without ischemic heart disease. *Am Heart J* 1987;114:84–90.
11. Tamaki S, Nakajima H, Murakami T, et al. Estimation of infarct size by myocardial emission computed tomography with thallium-201 and its relation to creatine kinase-MB release after myocardial infarction in man. *Circulation* 1982;66(5):994–1001.
12. Verani MS, Jeroudi MO, Mahmarian JJ, et al. Quantification of myocardial infarction during coronary occlusion and myocardial salvage after reperfusion using cardiac imaging with technetium-99m hexakis 2-methoxyisobutyl isonitrile. *J Am Coll Cardiol* 1988;12:1573–1581.
13. Gibbons RJ, Verani MS, Behrenbeck T, et al. Feasibility of tomographic ^{99m}Tc-hexakis-2-methoxy-2-methylpropyl-isonitrile imaging for the assessment of myocardial area at risk and the effect of treatment in acute myocardial infarction. *Circulation* 1989;80:1277–1286.
14. Weiss ES, Ahmed SA, Welch MJ, Williamson JR, Ter-Pogossian MM, Sobel BE. Quantification of infarction in cross sections of canine myocardium in vivo with positron emission transaxial tomography and ^{11}C-palmitate. *Circulation* 1977;55:66–73.
15. Ter-Pogossian MM, Klein MS, Markham J, Roberts R, Sobel BE. Regional assessment of myocardial metabolic integrity in vivo by positron-emission tomography with ^{11}C-labeled palmitate. *Circulation* 1980;61: 242–255.
16. Gould KL, Yoshida K, Hess MJ, Haynie M, Mullani N, Smalling RW. Myocardial metabolism of fluorodeoxyglucose compared to cell membrane integrity for the potassium analogue rubidium-82 for assessing infarct size in man by PET. *J Nucl Med* 1991;32:1–9.
17. Krivokapich J, Smith GT, Huang SC, et al. Nitrogen-13-ammonia myocardial imaging at rest and with exercise in normal volunteers. *Circulation* 1989;80:1328–1337.
18. Nienaber CA, Ratib O, Gambhir SS, et al. A quantitative index of regional blood flow in canine myocardium derived noninvasively with ^{13}N ammonia and dynamic positron emission tomography. *J Am Coll Cardiol* 1991; 17:260–269.
19. Fischbein MC, Meerbaum S, Rit J, et al. Early phase acute myocardial infarct size quantification: validation of the triphenyltetrazolium chloride tissue enzyme staining technique. *Am Heart* 1981;101:593–600.
20. Ashkar GP, Modestino JW. The contour extraction problem with biomedical applications. *Comp Graphics Image Proc* 1978;7:331–335.
21. Reiber JHC, Lie SP, Simoons ML, et al. Clinical validation of fully automated computation of ejection fraction from gated equilibrium blood-pool scintigrams. *J Nucl Med* 1983;24:1099–1107.
22. Hashimoto T, Kambara H, Fudo T, et al. Non-Q wave versus Q wave myocardial infarction: regional myocardial metabolism and blood flow assessed by positron emission tomography. *J Am Coll Cardiol* 1988;12: 88–93.
23. Hoffman EJ, Huang SC, Phelps ME. Quantitation in positron emission tomography: 1. Effect of object size. *J Comput Assist Tomogr* 1979;3: 299–308.
24. Marcassa C, Marzullo P, Parodi O, Sambuceti G, L'Abbate A. A new method for noninvasive quantitation of segmental myocardial wall thickening using technetium-99m-2-methoxy-isobutyl-isonitrile scintigraphy — results in normal subjects. *J Nucl Med* 1990;31:173–177.
25. Hoffman EJ, Phelps ME, Wisenberg G, Schelbert HR, Kuhl DE. Electrocardiographic gating in positron emission computed tomography. *J Comput Assist Tomogr* 1979;3:733–739.
26. Yamashita K, Tamaki N, Yonekura Y, et al. Quantitative analysis of regional wall motion by gated myocardial positron emission tomography: validation and comparison with left ventriculography. *J Nucl Med* 1989; 30:1775–1786.